Charge transport perpendicular to the high mobility plane in organic crystals: Bandlike temperature dependence maintained despite hundredfold anisotropy

B. Blülle,[1,*] A. Troisi,[2] R. Häusermann,[3] and B. Batlogg[1]
[1]*Laboratory for Solid State Physics, ETH Zurich, 8093 Zurich, Switzerland*
[2]*Department of Chemistry and Centre for Scientific Computing, University of Warwick, Coventry CV4 7AL, United Kingdom*
[3]*Department of Advanced Materials Science, The University of Tokyo, Chiba 277-8561, Japan*
(Received 20 October 2015; revised manuscript received 15 December 2015; published 28 January 2016)

Charge carrier mobility in van der Waals bonded organic crystals is strongly dependent on the transfer integral between neighboring molecules, and therefore the anisotropy of charge transport is determined by the molecular arrangement within the crystal lattice. Here we report on temperature dependent transport measurements along all three principal crystal directions of the same rubrene single crystals of high purity. Hole mobilities are obtained from the carrier transit time measured with high-frequency admittance spectroscopy perpendicular to the molecular layers (μ_c) and from the transfer characteristics of two field-effect transistor (FET) structures oriented perpendicularly to each other in the layers (μ_a and μ_b). While the measurements of the field-effect channels confirm the previously reported high mobility and anisotropy within the *ab* plane, we find the mobility perpendicular to the molecular layers in the same crystals to be lower by about two orders of magnitude ($\mu_c \sim 0.2\ \mathrm{cm}^2/\mathrm{Vs}$ at 300 K). Although the bandwidth is vanishingly small along the *c* direction and the transport cannot be coherent, we find μ_c to increase upon cooling. We show that the delocalization within the high mobility *ab* plane prevents the formation of small polarons and leads to the observed "bandlike" temperature dependence also in the direction perpendicular to the molecular layers, despite the incoherent transport mechanism.

DOI: 10.1103/PhysRevB.93.035205

I. INTRODUCTION

Understanding the charge transport physics in organic molecular semiconductors on a microscopic scale remains one of the central aspects for exploring those new electronic materials. Since the discovery of their semiconductivity in the forties [1,2], a variety of models and theories have been discussed to explain the experimentally investigated electronic properties of these van der Waals bonded compounds [3–6]. In recent studies, one particular observation appears to be a central element: Molecules in a crystal are not static and rigid entities, since the weak bonding allows the molecules to fluctuate about their position and relative orientation in the crystal lattice [7]. This thermally driven or zero-point motion dynamically modulates the transfer integral given by the weak overlap between the highly oriented π orbitals and leads to off-diagonal electronic disorder [8–11].

Almost without exception, molecules in organic semiconducting crystals are arranged in layers with strong electronic coupling and high charge mobility within these layers. The theories of transport in molecular crystals introduced over the past decade [12] mainly apply to the high mobility plane, and it has not yet been established how charge transport should be described in the direction perpendicular to this plane. Along this direction, where the mobility is expected to be strongly reduced, the charge carrier needs to cross the weak end-to-end bonds of the molecules, coupled by a transfer integral not exceeding few meV, two orders of magnitude smaller than the transfer integral within neighboring molecules in the high mobility plane. It is therefore interesting to assess whether the transport mechanism in the direction perpendicular to the high mobility plane takes place through a different mechanism and how this mechanism is influenced by the transport within molecular layers. Thus, measuring the temperature dependent mobility along these main directions provides important insights into the nature of charge transport in crystals of highly anisotropic molecule stacking.

Rubrene is an excellent example to study the transport in "layered" molecular crystals: Within the molecular layers the hole mobility is exceptionally high [13,14] and field-effect measurements in various directions within the *ab* plane of the same crystal have shown that μ_b is typically 2–4 times larger than μ_a [14–16], obeying the same "bandlike" temperature dependence upon cooling [14]. On the other hand, mobilities of the order $\mu_c \sim 0.3\ \mathrm{cm}^2/\mathrm{Vs}$ have been reported from photo-induced time-of-flight measurements perpendicular to the molecular planes [17,18]. To elucidate and quantify the apparent large anisotropy of charge transport in rubrene, we measure in this study the hole transport and its temperature dependence in all principle crystal directions simultaneously in the same crystal.

II. MOBILITY IN THREE PRINCIPLE CRYSTAL DIRECTIONS OF RUBRENE

The measurement of the in-plane and out-of-plane mobility in the same sample requires a combination of measurement techniques: A platelet-shaped, $\sim 2\,\mu$m thick orthorhombic rubrene crystal is laminated on top of a ready-made FET structure with channels parallel to *a* and *b*. Then we add a third channel along *c* by laminating an additional electrode on top of the crystal, forming an electrode-semiconductor-electrode "sandwich" structure. A photograph of one of the samples is shown in Fig. 1.

The mobility μ_c is obtained from admittance spectroscopy, measuring the frequency dependent response of the current

*bbluelle@phys.ethz.ch

 ©2016 American Physical Society

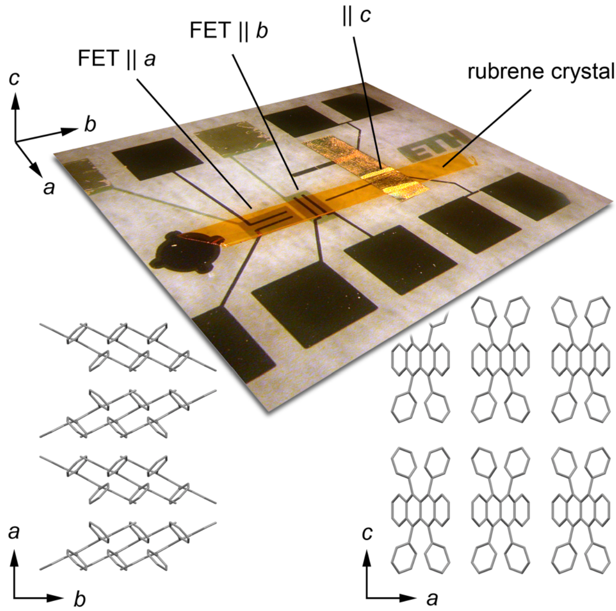

FIG. 1. Optical photograph of sample 1 consisting of two perpendicular FET channels with Cytop as gate dielectric and two laminated electrodes on top/bottom of the crystal forming a vertical channel. The ribbon-shaped rubrene crystal was laminated such that the a and b axis are aligned with the source-drain directions of the FETs. The stacking order of the rubrene molecules leads to the highest orbital overlap in the b direction, for which the largest mobility was measured. The same device geometry was used for samples 2 and 3.

upon an applied AC field. When an additional DC bias voltage is applied, the finite charge carrier transit time leads to an oscillatory feature in the high frequency range of the conductance spectrum, which is in direct relation to μ_c [19,20]. Charge mobilities along the a and b directions are determined from the saturation regime of the FET transfer curves. More details about device fabrication, measurement procedure, and data analysis are discussed in the experimental section.

Figure 2 shows the results from three samples, where the temperature dependent measurement in three directions on the same crystal was successful. We find μ_c to be about 10^2 times smaller than $\mu_{a,b}$, revealing a very strong timescale separation between the carrier dynamics in the ab plane and in the perpendicular c direction. Remarkably, we find for μ_c a very similar temperature dependence as for the in-plane charge transport, i.e., increasing upon cooling, despite its much smaller absolute value.

III. MODELING OF THE IN-PLANE AND OUT-OF-PLANE CHARGE TRANSPORT

Although rubrene exhibits very high mobilities of the order of 10 cm^2/Vs along the molecular layers with a bandlike temperature dependence, the charge motion is not compatible with band transport because the mean free path of the carrier would be too short (shorter than the unit cell). On the other hand it is also incompatible with nearest neighbor hopping transport because the hopping time would have to be too fast (~0.1 ps), i.e., faster than vibrational relaxation [12,21]. The models proposed to deal with the high mobility plane describe the charge as moving coherently but subject to a very strong coupling with low frequency modes of the crystal that cause dynamic disorder [5] or transient localization [22]. In practice, the transfer integral between nearest neighbors is dynamically modulated by fluctuations on the timescale of ~1 ps with an amplitude comparable to the average value of the transfer integral.

As mentioned before, our experimental data reveal a clear separation between the carrier dynamics in the ab plane and in the perpendicular c direction. The measured transport in the c direction is definitely too slow to be coherent but becomes compatible with an incoherent hopping mechanism.

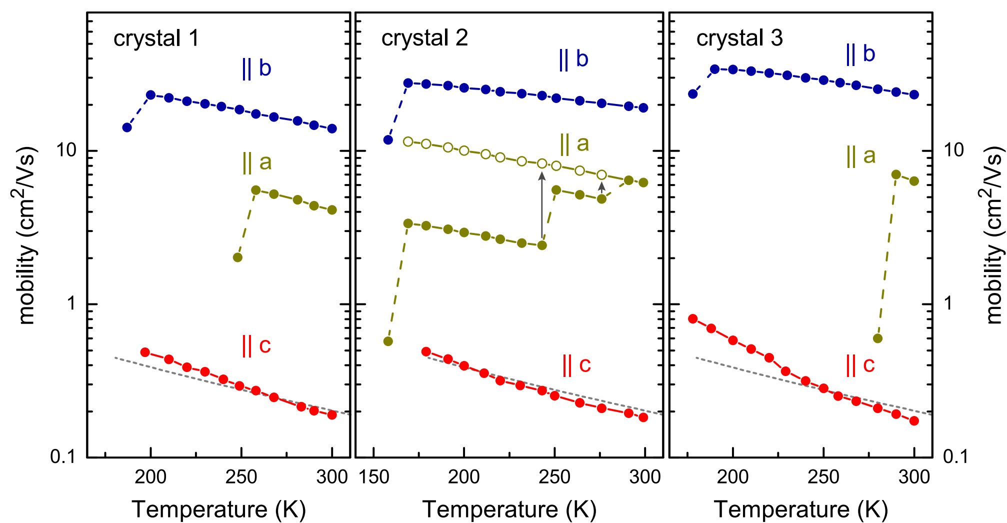

FIG. 2. Hole mobility in rubrene in all three principle crystal directions as a function of temperature. All the mobilities are measured simultaneously and increase towards lower temperatures, although the charge transport is highly anisotropic, i.e., μ_c is $\sim 10^2$ times smaller than μ_b. The formation of cracks leads to an apparent discontinuous drop of μ and for sample 2, the μ_a curves are shifted correspondingly. For comparison, the gray dashed line shows the modeled temperature dependence of μ_c, assuming a charge transfer integral $t_c = 0.9$ meV and including the wave function delocalization within the ab planes.

Considering the interlayer distance of 13.5 Å, a mobility $\mu_c \sim 0.2\,\mathrm{cm}^2/\mathrm{Vs}$ implies a room temperature hopping time τ_h between layers of ∼3 ps, as estimated from Einstein's relation $\mu = L^2 e/\tau_h k_B T$. The dynamics within the *ab* plane is so much faster that the hopping events along the *c* direction can be considered uncorrelated from each other (i.e., incoherent). On this timescale of diffusion along the *c* direction one can assume that the carriers are equilibrated within each *ab* layer.

Electronic structure calculations are fully consistent with this view of rubrene as formed by very weakly interacting *ab* planes. We have recomputed the average transfer integral and its thermal fluctuations with the method of Ref. [23] but with an improved DFT level (B3LYP/6-31g*) to increase accuracy on the challenging coupling along the *c* direction and to be better aligned with more recent similar works [24]. We computed the coupling along the *a*, *b*, and *c* directions to be 21, 140, and −2.7 meV, in agreement with band structure calculations [25]. Thermal motions cause a fluctuation of these values at 300 K comparable to their average value and computed to be 10, 40, and 1.3 meV, respectively. To an excellent degree of approximation the fluctuation of the transfer integral is proportional to the square root of the temperature [26] and is therefore easy to evaluate for the range of temperatures considered experimentally.

In the following we explore to what degree charge transport perpendicular to the molecular layers is affected by in-plane transport. We proceed quantitatively by assuming that the carrier moves incoherently between *ab* layers, find the transfer matrix element that reproduces the experimental data, and then compare it with the electronic structure results. In this way we ensure that the transport model, electronic structure calculation, and experimental data are fully consistent.

The rate of hopping from one initial state $|i_1\rangle$ in layer 1 to any another state $|j_2\rangle$ in adjacent layer 2 can be given by the Fermi golden rule:

$$k_{i_1} = \frac{2\pi}{\hbar} \sum_{j_2} |\langle i_1|H|j_2\rangle|^2 \delta(E_{i_1} - E_{j_2}). \quad (1)$$

E_{i_1} and E_{j_2} are the energies of the noninteracting layers, H the electronic Hamiltonian, and δ the Dirac delta. Because of the timescale separation discussed above we assume that the equilibration within a given layer is rapidly established with respect to the interlayer hopping, and the average hopping rate can be defined as $1/\tau_h = k_h = \sum_{i_1} P(i_1,T,n)k_{i_1}$, where $P(i_1,T,n)$ is the population of state i_1 at a given temperature and charge density n. The equation implies a purely electronic process because the charges are too delocalized for local electron-phonon coupling terms to be important. In other words, this model of the charge dynamics in the *ab* direction incorporates two elements, namely the charge dynamics along *ab* being much faster than along *c* and the carriers in the *ab* plane being sufficiently delocalized (e.g., over more than 10 molecules). The mobility is obtained from the hopping rate using Einstein's relation.

The eigenstates of the *ab* plane of rubrene, including the effect of thermal disorder, are calculated at 200 and 300 K following the procedure described in Ref. [27]. These states represent the initial and final states of Eq. (1).

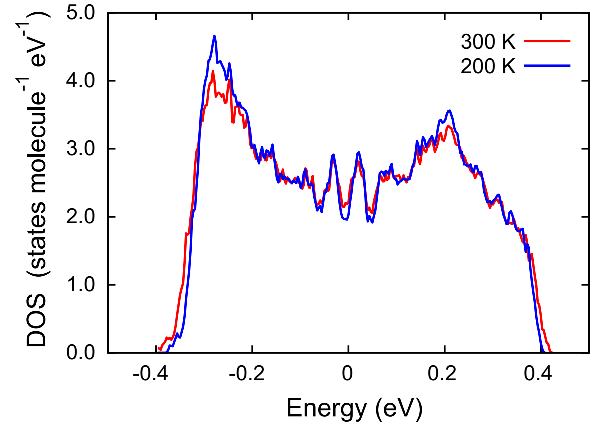

FIG. 3. Density of states (DOS) in the highest occupied band computed for the dynamically disordered *ab* plane of rubrene at 300 and 200 K.

To compute the hopping rate k_h we consider layers of 30×30 unit cells with periodic boundary conditions and average over 64 realizations of disorder. This model includes the calculated density of states (DOS) for the highest occupied band, as given in Fig. 3, and the disorder in adjacent layers is assumed to be uncorrelated. The hopping process can be visualized as in the cartoon of Fig. 4, where an initial state located on a layer hops to one of the states at equal energy in the adjacent layer that is located approximately in the same region. We have noted that there is little influence of the charge density on the hopping rate, and we therefore report the results

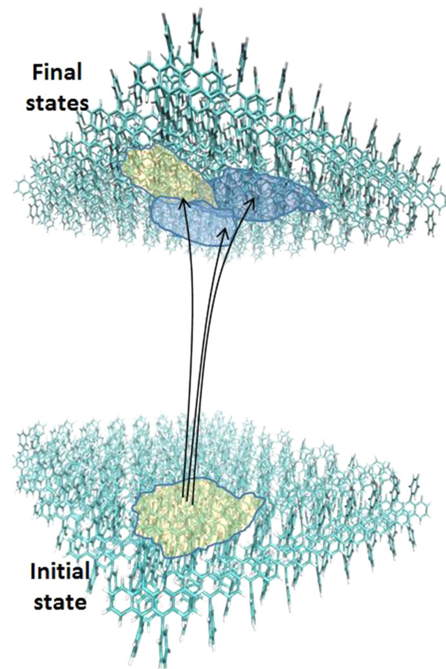

FIG. 4. Visualization of the charge hopping between two adjacent rubrene molecule layers. The hopping rate is given by the Fermi golden rule. Within the layers the wave function is spread out over many molecules, and charge transfer takes place on a much faster timescale than from layer to layer.

in the limit of vanishing density. Also the temperature has a very small effect on k_h: The hopping rate decreases by a factor of 0.78 when the temperature is increased from 200 to 300 K.

The matrix elements $\langle i_1|H|j_2\rangle$ are computed expanding $|i_1\rangle$ and $|j_2\rangle$ as a linear combination of rubrene HOMO orbitals $|l_1\rangle$ and $|m_2\rangle$ localized on isolated molecules in two adjacent layers. The coupling $\langle l_1|H|m_2\rangle$ is set to the transfer integral t_c if the molecules are in contact or to zero otherwise. As $|t_c|^2$ appears as a prefactor of the hopping rate, it affects the absolute value of the mobility but not the temperature dependence. The measured mobilities of 0.2 $\mathrm{cm^2/Vs}$ at RT and $\sim$0.5 $\mathrm{cm^2/Vs}$ at 200 K can be reproduced by this model using a transfer integral t_c of 0.9 meV and t_c of 1.1 meV, respectively, which is three times smaller than the value computed by DFT and reported above. Considering the intrinsic inaccuracies of quantum chemistry coupling between very weakly interacting pairs and the simplicity of the model, this level of agreement is gratifying and no change in transport physics is expected within the variability of the parameters. Thus, the essential transport physics appears to be captured in our model.

As the hopping rate depends only weakly on T, the main source of temperature dependence of the mobility is the $1/T$ factor that connects the diffusion coefficient and the mobility. The model yields a mobility increase by a factor of 1.9 when going from 300 to 200 K. This is again in agreement with our measurements (2.5, 2.2, and 3.3 for the three crystals).

The straightforward approach for the charge transport dynamics perpendicular to the planes does not include any polaronic effect, and it is therefore important to compare it with alternative models and explanations of decreasing mobility with increasing temperature. In terms of an incoherent series of hopping between states localized on individual molecules, the hopping rate within Marcus theory would be given by [28]

$$k = \frac{2\pi}{\hbar}|t_c|^2(4\pi\lambda k_B T)^{-\frac{1}{2}} \exp\left(-\frac{\lambda}{4k_B T}\right), \qquad (2)$$

where λ is the reorganization energy of the crystal. For the case of rubrene, $\lambda \sim 156$ meV [29] (typical for other organic crystals), this would correspond to an increasing mobility with temperature up to room temperature ($\mu_{\max}$ at $T = \lambda/6k_B$), at variance with the observation.

Considering, however, the delocalization of the charge wave function over n molecules within the layers, the hopping process between two states at energies $E_{i,1}$ and $E_{j,2}$ in adjacent layers would lead to a hopping rate [30]

$$k = \frac{2\pi}{\hbar}|\langle i_1|H|j_2\rangle|^2(4\pi\lambda k_B T/n)^{-\frac{1}{2}} \times \exp\left(-\frac{(\lambda/n + E_{j,2} - E_{i,1})^2}{4(\lambda/n)k_B T}\right). \qquad (3)$$

In the case of a pronounced delocalization (i.e., for sufficiently large n) this expression becomes identical to the Fermi golden rule [Eq. (1)], since the last two factors converge to $\delta(E_{j,2} - E_{i,1})$ as $n \to \infty$. Therefore, our model for the mobility in the c direction can be seen as the limit of a small polaron model when the delocalization within the ab plane becomes sufficiently large. In this limit, the mobility along the c direction becomes insensitive to the value of λ and will not be modified if we adopt more complicated polaronic hopping expressions that consider, e.g., the quantum nature of the nuclear modes that cause the formation of the small polaron [31].

The incoherent hopping between weakly coupled molecular layers within which band transport takes place was also addressed by Sumi [32], expanding on an earlier work by Gosar and Choi [33]. They assumed band transport in the plane with larger bandwidth and obtained an expression of the mobility which is the sum of two contributions, a hopping term obtained from the golden rule and a phonon induced conductivity. In contrast to our study, the first contribution is based on total momentum conserving band states and decreases very rapidly with temperature, i.e., should be negligible at room temperature. The phonon induced contribution gives a temperature independent mobility, essentially because the coupling element in the golden rule, proportional to the temperature in Sumi's model, is compensated by the $1/T$ factor connecting hopping rates and mobility. These theories cannot be used in the case of organic molecular crystals, because the assumption of band transport in the ab plane is not consistent with our current understanding of charge transport in these materials, and it is not surprising that they disagree with the observation of $\mu \propto T^{-n}$ ($n \approx 1-2$). However, these studies are relevant here because the problem was formulated in a very similar way at a time when the effect of dynamic localization was not known.

IV. DEVICE FABRICATION AND MOBILITY MEASUREMENT

We have built samples with conductive channels in all crystal directions by laminating a rubrene single crystal onto a ready-made transistor structure (FETs a and b) and covering one end of the crystal by an additional electrode for out-of plane measurements (c direction). The substrate is based on 0.5 mm thick borosilicate glass on which we thermally evaporated through a shadow mask a Cr/Au film (1 nm/10 nm) as structured gate for the transistor channels, covered by a Cytop layer as gate dielectric [34]. Cytop CTL-809M mixed with the solvent CT-Solv-180 in a 3:2 ratio and spin coated at 500 rpm for 10 s and 1000 rpm for 30 s resulted in a 480 nm thick film, which was cured at 120° C for 1 h. Evaporated Au (35 nm) is used as the bottom contact of the SCLC channel and as source/drain electrodes for the FETs, forming two 80 μm long perpendicularly oriented channels.

Rubrene powder (98% purity, Sigma Aldrich) served as source material to grow orthorhombic single crystals by physical vapor transport in an Ar flux [35]. The ribbon-shaped crystals studied here are $\sim$5 mm long, $\sim$0.5 mm wide, and $\sim$2 μm thick and were attached to the prefabricated substrate by spontaneous adhesion such that the crystalline directions a and b are aligned with their corresponding FET channels. Then, we laminated an elastic strip of PDMS with a sputtered 30 nm Au layer on top, forming an overlapping region with the bottom contact to measure charge transport in the c direction.

The samples are mounted on a homemade setup for temperature dependent measurements, with cabling and shielding optimized for low-noise DC analysis and impedance spectroscopy at high frequencies (up to 100 MHz), and all measurements were carried out in dark and in Ar atmosphere. Current-voltage characteristics of the transistor channels were

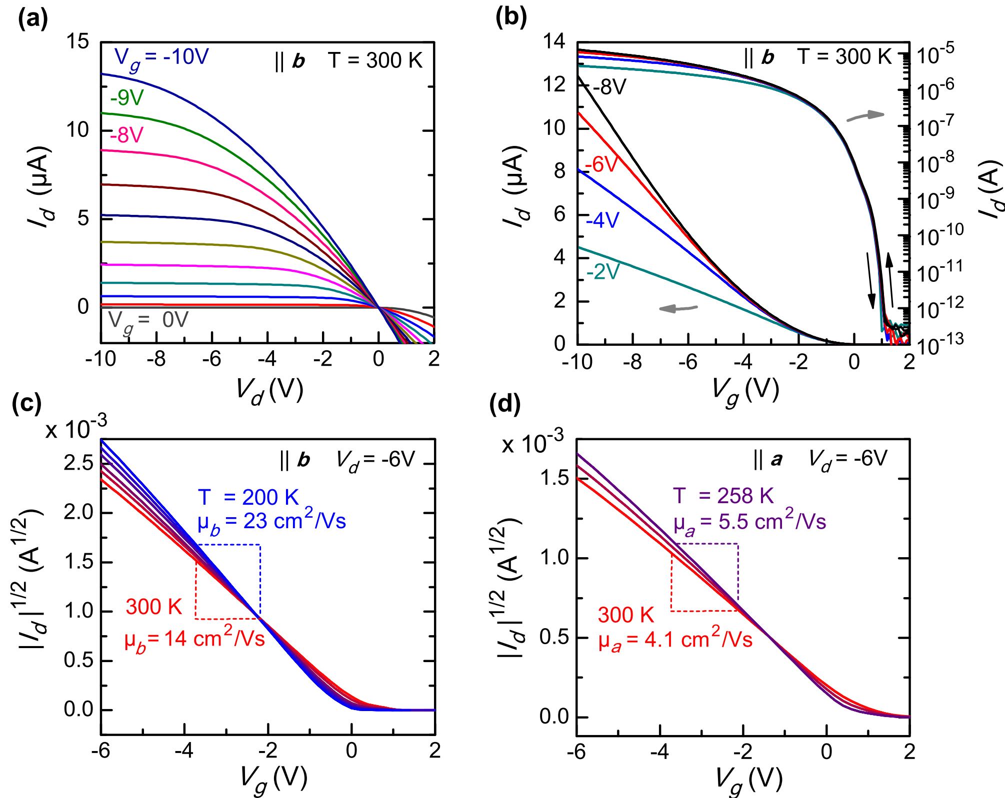

FIG. 5. FET characteristics of crystal 1 to determine μ_a and μ_b: (a) The output curves, here shown for the b direction at 300 K, have a linear zero crossing, i.e., the drain current is not contact limited. (b) The transfer characteristics exhibit a steep subthreshold slope ($S \sim 0.1$ V/dec) and no hysteresis, indicating a low density of trap states. (c),(d) In both the b and a direction the slope of the square root of I_d increases upon cooling due to higher mobilities at lower temperatures.

measured using a HP 4156A semiconductor parameter analyzer, and an Agilent 4294 impedance analyzer was used for conductance spectroscopy in the c direction. We gradually cooled the samples with LN_2 from RT down to $\sim$160 K, and measurements were taken every $\sim$10 K. Upon cooling, cracks develop parallel to b due the anisotropic thermal expansion of rubrene ($\Delta^a_{\text{Rub}} = 7.8 \times 10^{-5}\,\text{K}^{-1}$, $\Delta^b_{\text{Rub}} = 1.6 \times 10^{-5}\,\text{K}^{-1}$) [36] on top of the borosilicate/cytop substrate with a smaller and isotropic expansion coefficient ($\Delta_{\text{glass}} = 7.2 \times 10^{-6}\,\text{K}^{-1}$). This cracking is typically observed between 280 and 250 K.

A. Mobility in the *a* and *b* direction, along the layers

The field-effect channels in the a and b direction show similar electrical characteristics: The linear zero crossing (no S shape) of the output curves [shown in Fig. 5(a) for FET $\parallel b$] indicates a low charge injection barrier at the contacts and justifies the extraction of the mobility from a two-point measurement. The transfer characteristics [Fig. 5(b)] exhibit a steep subthreshold slope, no hysteresis, very low gate leakage currents, and a turn-on close to 0 V, similar to the high quality devices in Ref. [37]. Here, we extract the mobility from the saturation regime ($|V_g| < |V_d|$), where μ_{sat} is given by the slope of the square root of the saturation current I_d versus gate voltage V_g,

$$\mu_{\text{sat}} = \frac{2L}{WC}\left(\frac{\partial\sqrt{I_d}}{\partial V_g}\right)^2, \tag{4}$$

with L and W the FET channel length and width, respectively, and C is the gate capacitance. Figures 5(c) and 5(d) show the measured slope of $\sqrt{I_d}$ vs V_g in the b and a direction to increase upon cooling, corresponding to a mobility increase of μ_b from 14 cm^2/Vs to 23.1 cm^2/Vs for a change in T from 300 to 200 K, and from $\mu_a = 4.1$ cm^2/Vs at 300 K to 5.5 cm^2/Vs at 258 K. Very similar results are obtained for crystals 2 and 3 (see Fig. 2).

B. Mobility in the *c* direction, perpendicular to the layers

Charge transport in the c direction is measured by admittance spectroscopy: By sweeping the frequency of an AC voltage $\tilde{V}\exp(i\omega t)$ superimposed on an applied DC field $E \approx V_0/t_{sc}$, the average transit velocity is obtained from oscillatory features in the complex response of the current $\tilde{I}\exp(i\omega t)$. Such transit time oscillations are directly related to the drift mobility and have first been observed in silicon microwave diodes [38]. In the past decade, admittance spectroscopy has become a well-established method to measure the mobility also in organic semiconductors and is a powerful alternative to the time-of-flight (TOF) technique, with no necessity of optically generating charge carriers with a laser pulse and thus suited even for very thin semiconductors [19,20,39–41].

The crystals studied here are contacted with a bottom and top electrode, forming a sandwichlike planar device structure for which charge transport can be parametrized using the well-known formalism of space-charge limited current (SCLC)

in one dimension. Considering p-type transport in rubrene, assuming that the gold contacts are ohmic and neglecting thermal diffusion, the current density j as a function of the electric field E is given by the drift and the displacement current,

$$j(x,t) = q\mu\rho(x,t)E(x,t) + \varepsilon_{sc}\frac{\partial E(x,t)}{\partial t}, \quad (5)$$

where μ is the hole mobility and ε_{sc} the permittivity of the semiconductor. The local density of charge carriers, $\rho(x,t)$, is related to the electric field by Poisson's equation $\partial E(x,t)/\partial x = q\rho(x,t)/\varepsilon_{sc}$.

Considering perturbations up to first order, $\kappa = \kappa_0 + \tilde{\kappa}\exp(i\omega t)$, where κ stands for the quantities $V(t)$, $j(t)$, $E(x,t)$, and $\rho(x,t)$, the AC component of the current density can be written as [20]

$$\tilde{j}(t) = \left(q\mu\rho_0\tilde{E} + \varepsilon_{sc}\mu E_0\frac{\partial\tilde{E}}{\partial x} + i\omega\varepsilon_{sc}\tilde{E}\right)\exp(i\omega t), \quad (6)$$

where the first term corresponds to the response of the steady-state charge distribution to the applied AC field, a second contribution is given by the currents of an additionally injected time-dependent charge carrier density, and the third term is the displacement current through the semiconductor seen as an ideal dielectric.

As a function of the frequency ω, the complex admittance $Y(\omega) = \tilde{j}/\tilde{V}$ reads [38,42]

$$Y(\omega) = \mu\frac{i\omega^3}{j_0} \times \frac{1}{i\omega\tau + e^{-i\omega\tau} + \frac{\omega^2\tau^2}{2} - 1}, \quad (7)$$

describing the first order small signal response of the SCLC current to a small AC signal $\tilde{V}$. The admittance is commonly represented by the conductance and capacitance spectrum, G and C, with $Y(\omega) = G + i\omega C$. The quantity of most relevance in this study is the transit time τ, because it is inversely proportional to the mobility according to [41,42]

$$\tau = \frac{4}{3}\frac{d^2}{(V_0 - V_{\mathrm{bi}})\mu}, \quad (8)$$

where $V_0 - V_{\mathrm{bi}}$ is the applied bias reduced by the built-in voltage.

The blue curve in Fig. 6 shows the small signal conductance $G(f) = \mathrm{real}(Y(f))$ given by Eq. (7), exhibiting oscillatory characteristics above $f \sim 1/\tau$, with a first negative peak at $f_t = 1.16/\tau$. The extraction of f_t directly yields the average transit time τ and therefore the charge carrier mobility μ according to Eq. (8).

Equation (7) and its minimum in $G(f)$ at $f_t = 1.16/\tau$ are a result of the $T = 0$ approximation, where diffusion is neglected. We therefore verify the validity of the mobility extraction at finite temperatures by also considering the diffusion current $j_{\mathrm{diff}} = -qD\,\partial\rho(x,t,)/\partial x$ with $D = k_BT\mu$ in a numerical calculation of the drift-diffusion equations upon an AC small signal perturbation. These simulations for different temperatures are shown in Fig. 6(a) (yellow to red curves) and yield a slight reduction (damping) of higher order oscillations at high temperatures, while for $T \to 0$ K we obtain the same result as from the analytical expression. Reassuringly, for finite temperatures the first peak at f_t is only slightly shifted towards

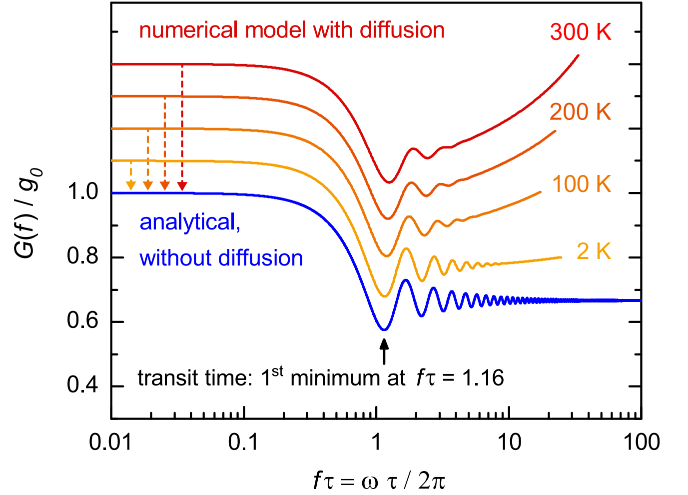

FIG. 6. Modeled theoretical small signal conductance of an ideal semiconductor structure sandwiched between two ohmic contacts. The analytical model (blue curve) corresponds to Eq. (6) and neglects diffusion currents. For comparison, we added a numerical solution for finite temperatures, including diffusion (yellow to red curves). All curves exhibit a first negative peak at $f\tau \sim 1.16$, yielding a relation between the transit time τ and the frequency, at which the oscillation occurs.

higher frequencies, by at most 7% between 0 and 300 K. Therefore, the relative uncertainty of the extracted mobility due to diffusion is less than 3% in the temperature range of the measured data presented here.

Figure 7(b) shows the measured small signal conductance $G(f)$ of crystal 1 at 300 K for different bias voltages. At low frequencies, the AC conductance corresponds to the DC incremental conductance $g_0 = \frac{\partial I_{dc}}{\partial V_{dc}}$, i.e., the slope of the steady-state IV characteristics which is determined by the density of trap states in the band gap [43,44]. The conductance slightly increases towards higher frequencies due to a reduction of charge capture by slow traps with decreasing measure period [45–47]. At high frequencies, where the oscillation period of the AC signal becomes shorter than the charge carrier transit time from the injecting to the extracting electrode, the conductance signal is abruptly suppressed with a negative peak f_t, shown as black triangles in Fig. 7(a).

For comparison we show in Fig. 7(b) the numerical solution of the time-dependent drift and diffusion equations of a trap-free semiconductor with $\mu = 0.1$ cm^2/Vs at 300 K at several bias voltages. These calculations do not involve any data fitting, and the remarkable qualitative agreement between measured and modeled AC conductance spectrum is a further indication that highly pure rubrene crystals behave like ideal textbook semiconductors. Importantly, the mobility μ, here related to the transit oscillations, corresponds to the drift mobility, i.e., is equivalent to the DC mobility obtained from steady-state measurements. Therefore, the μ_c perpendicular to the molecule layers measured with admittance spectroscopy is fully compatible with the in-layer mobilities μ_a and μ_b we obtain from FET measurements, since both methods are based on the same set of differential equations describing the macroscopic charge dynamics.

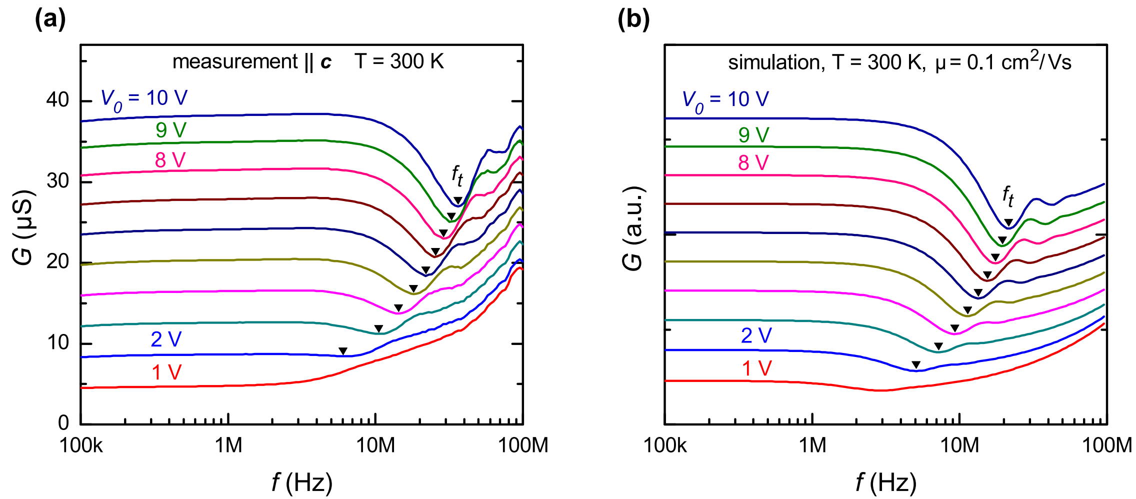

FIG. 7. Mobility measurement in the c direction of crystal 1 using admittance spectroscopy: (a) Measured conductance spectrum at 300 K for several bias voltages V_0, using a fixed AC voltage $V_{\mathrm{ac}} = 0.2$ V, yielding textbooklike transit oscillations with first negative peaks f_t between 6 and 40 MHz. (b) For comparison: Modeled conductance spectrum of an ideal trap-free semiconductor at 300 K with a mobility of 0.1 cm^2/Vs. We obtain these results by numerically solving the drift-diffusion equations [Eq. (5) + diffusion term], using only mobility, temperature, and geometry as input parameters, without any data fitting.

From the measured conductance spectrum (Fig. 7) we extract the transit time as a function of the applied bias voltage using $\tau \sim 1.16/f_t$, which directly yields the mobility. Figure 8 shows the transit frequencies f_t from the conductance spectra measured at different temperatures. Upon cooling, the transit oscillations move towards higher frequencies, corresponding to shorter transit times, i.e. higher mobilities. For all measured temperatures f_t grows linearly with V_0, while the zero crossing is slightly shifted from $\sim$0 V at RT towards positive values at lower temperatures. Assuming that only a built-in voltage adds to the applied field, i.e., $E \approx (V_0 - V_{\mathrm{bi}})/t_{sc}$, the mobility can be obtained from the slope of $f_t(V_0)$, according to

$$\mu = \frac{4}{3}\frac{d^2}{1.16}(\partial f_t/\partial V_0), \tag{9}$$

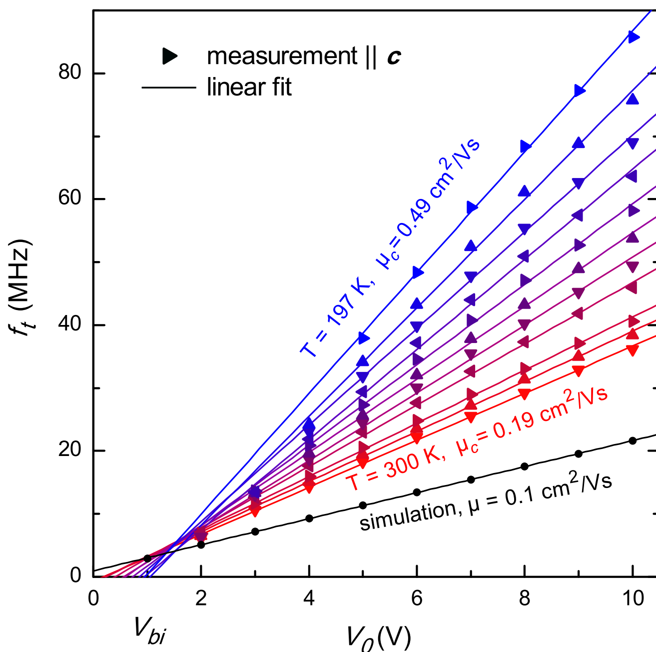

FIG. 8. Bias dependence of the transit frequencies f_t measured on crystal 1 at different temperatures. The mobility μ_c is calculated from the slope of $f_t(V_0)$ and increases with decreasing temperature. The linearity of $f_t(V_0)$ is a sign for field-independent mobility. The transit frequencies obtained from the simulations for $\mu = 0.1$ cm^2/Vs (see Fig. 7) are shown for comparison.

yielding $\mu_c = 0.19$ cm^2/Vs at 300 K to 0.49 cm^2/Vs at 197 K for crystal 1 and very similar values for crystals 2 and 3 (see Fig. 2). The linear relation of $f_t(V_0)$ indicates that the measured mobility is field independent.

V. CONCLUSION

In conclusion we have measured the mobility in the three principle crystal directions of the organic semiconductor rubrene in the temperature range of 300 to 170 K. These simultaneous transport measurements in different directions on the same crystals involve a combination of two FET channels with an additional metal-semiconductor-metal structure, for which mobilities can be extracted from the FET transfer characteristics in the a and b direction and from admittance spectroscopy across the molecular layers (c direction). By comparing the measured admittance spectra to a time-dependent numerical solution of the drift-diffusion equations, we have ensured that the mobility μ_c obtained from transit-time oscillations in the AC spectrum is fully compatible with the field mobility extracted from the FET transfer curves. Furthermore, the linear relationship of the measured transit times in the c direction with respect to the applied DC bias voltage is an indication of field-independent charge transport.

The layered molecular structure of the orthorhombic rubrene crystals manifests itself in a highly anisotropic transport dynamics, associated with a clear timescale separation between charge transport within the layers and perpendicular

to them. In three samples we have measured the charge carrier transit times in the c direction which correspond to a mobility $\mu_c = 0.2\ \mathrm{cm}^2/\mathrm{Vs}$ at room temperature. These values are $\sim 10^2$ times smaller than the mobilities along the a and b direction of the same crystals.

The observed "bandlike" temperature dependence of the in-plane transport is interpreted as coherent motion limited by dynamic disorder or transient localization. On the other hand, a very similar increase of the mobility upon cooling has been measured perpendicular to the layers, which at first glance seems contradictory to a thermally activated hopping transport that might have been expected due to the very small transfer integral across the layers and the high polaron formation energy.

Our experimental results, however, are quantitatively explained with a transport model that takes into account the difference in timescale between the transport in the ab plane and the c direction and involves incoherent hopping of the charge carrier between adjacent ab planes promoted by the very weak coupling between them. While the transport in the ab plane and along the c direction are effectively decoupled, the nature of the transport along c is determined by the degree of delocalization and, thus, the transport mechanism in the ab plane.

[1] D. D. Eley, Nature (London) **162**, 819 (1948).
[2] H. Akamatu and H. Inokuchi, J. Chem. Phys. **18**, 810 (1950).
[3] J. L. Brédas, J. P. Calbert, D. A. S. Filho, and J. Cornil, Proc. Natl. Acad. Sci. (PNAS) **99**, 5804 (2002).
[4] K. Hummer and C. Ambrosch-Draxl, Phys. Rev. B **72**, 205205 (2005).
[5] A. Troisi and G. Orlandi, Phys. Rev. Lett. **96**, 086601 (2006).
[6] S. Fratini and S. Ciuchi, Phys. Rev. Lett. **103**, 266601 (2009).
[7] A. Troisi, G. Orlandi, and J. E. Anthony, Chem. Mater. **17**, 5024 (2005).
[8] V. Coropceanu, R. S. Sánchez-Carrera, P. Paramonov, G. M. Day, and J. L. Brédas, J. Phys. Chem. C **113**, 4679 (2009).
[9] A. Troisi, Chem. Soc. Rev. **40**, 2347 (2011).
[10] V. Stehr, J. Pfister, R. F. Fink, B. Engels, and C. Deibel, Phys. Rev. B **83**, 155208 (2011).
[11] H. Ishii, N. Kobayashi, and K. Hirose, Phys. Rev. B **88**, 205208 (2013).
[12] S. Fratini, D. Mayou, and S. Ciuchi, arXiv:1505.02686.
[13] J. Takeya, M. Yamagishi, Y. Tominari, R. Hirahara, Y. Nakazawa, T. Nishikawa, T. Kawase, T. Shimoda, and S. Ogawa, Appl. Phys. Lett. **90**, 102120 (2007).
[14] V. Podzorov, E. Menard, A. Borissov, V. Kiryukhin, J. A. Rogers, and M. E. Gershenson, Phys. Rev. Lett. **93**, 086602 (2004).
[15] V. C. Sundar, J. Zaumseil, V. Podzorov, E. Menard, R. L. Willett, T. Someya, M. E. Gershenson, and J. A. Rogers, Science **303**, 1644 (2004).
[16] C. Reese and Z. Bao, Adv. Mater. **19**, 4535 (2007).
[17] W. G. Williams, Discuss. Faraday Soc. **51**, 61 (1971).
[18] T. J. Pundsack, N. O. Haugen, L. R. Johnstone, C. Daniel Frisbie, and R. L. Lidberg, Appl. Phys. Lett. **106**, 113301 (2015).
[19] H. C. F. Martens, H. B. Brom, and P. W. M. Blom, Phys. Rev. B **60**, R8489 (1999).
[20] S. W. Tsang, S. K. So, and J. B. Xu, J. Appl. Phys. **99**, 013706 (2006).
[21] A. Troisi, Organic Electronics **12**, 1988 (2011).
[22] S. Ciuchi, S. Fratini, and D. Mayou, Phys. Rev. B **83**, 081202 (2011).
[23] A. Troisi, Adv. Mater. **19**, 2000 (2007).
[24] A. S. Eggeman, S. Illig, A. Troisi, H. Sirringhaus, and P. A. Midgley, Nat. Mater. **12**, 1045 (2013).
[25] D. A. da Silva Filho, E.-G. Kim, and J.-L. Brédas, Adv. Mater. **17**, 1072 (2005).
[26] R. S. Sánchez-Carrera, P. Paramonov, G. M. Day, V. Coropceanu, and J.-L. Brédas, Jacs **132**, 14437 (2010).
[27] A. Troisi, J. Chem. Phys. **134**, 034702 (2011).
[28] R. A. Marcus, J. Chem. Phys. **24**, 966 (1956).
[29] S. Duhm, Q. Xin, S. Hosoumi, H. Fukagawa, K. Sato, N. Ueno, and S. Kera, Adv. Mater. **24**, 901 (2012).
[30] The reorganization energy is inversely proportional to the charge delocalization, see, e.g., A. Devos and M. Lannoo, Phys. Rev. B **58**, 8236 (1998).
[31] J. Jortner, J. Chem. Phys. **64**, 4860 (1976).
[32] H. Sumi, Solid State Commun. **28**, 309 (1978).
[33] P. Gosar and S.-I. Choi, Phys. Rev. **150**, 529 (1966).
[34] W. L. Kalb, T. Mathis, S. Haas, A. F. Stassen, and B. Batlogg, Appl. Phys. Lett. **90**, 092104 (2007).
[35] C. Kloc, P. Simpkins, T. Siegrist, and R. Laudise, J. Cryst. Growth **182**, 416 (1997).
[36] O. D. Jurchescu, A. Meetsma, and T. T. M. Palstra, Acta Crystallogr. Sect. B **62**, 330 (2006).
[37] B. Blülle, R. Häusermann, and B. Batlogg, Phys. Rev. Applied **1**, 034006 (2014).
[38] G. Wright, Solid-State Electron. **9**, 1 (1966).
[39] S. Berleb and W. Brütting, Phys. Rev. Lett. **89**, 286601 (2002).
[40] N. D. Nguyen, M. Schmeits, and H. P. Loebl, Phys. Rev. B **75**, 075307 (2007).
[41] S. Ishihara, H. Hase, T. Okachi, and H. Naito, Thin Solid Films **554**, 213 (2014).
[42] J. Shao and G. Wright, Solid-State Electron. **3**, 291 (1961).
[43] O. Zmeskal, F. Schauer, and S. Nespurek, J. Phys. C **18**, 1873 (1985).
[44] C. Krellner, S. Haas, C. Goldmann, K. P. Pernstich, D. J. Gundlach, and B. Batlogg, Phys. Rev. B **75**, 245115 (2007).
[45] D. Dascalu, Int. J. Electron. **21**, 183 (1966).
[46] R. Kassing, Phys. Status Solidi A **28**, 107 (1975).
[47] J. M. Montero, J. Bisquert, G. Garcia-Belmonte, E. M. Barea, and H. J. Bolink, Organic Electronics **10**, 305 (2009).